Front. Energy 2022, 16(4): 607–612
https://doi.org/10.1007/s11708-021-0798-0

RESEARCH ARTICLE

Cehuang FU, Shuiyun SHEN, Ruofei WU, Xiaohui YAN, Guofeng XIA, Junliang ZHANG

Facile controlled synthesis of hierarchically structured mesoporous $Li_4Ti_5O_{12}$/C/rGO composites as high-performance anode of lithium-ion batteries

Abstract In this paper, a facile strategy is proposed to controllably synthesize mesoporous $Li_4Ti_5O_{12}$/C nanocomposite embedded in graphene matrix as lithium-ion battery anode via the co-assembly of $Li_4Ti_5O_{12}$ (LTO) precursor, GO, and phenolic resin. The obtained composites, which consists of a LTO core, a phenolic-resin-based carbon shell, and a porous frame constructed by rGO, can be denoted as LTO/C/rGO and presents a hierarchical structure. Owing to the advantages of the hierarchical structure, including a high surface area and a high electric conductivity, the mesoporous LTO/C/rGO composite exhibits a greatly improved rate capability as the anode material in contrast to the conventional LTO electrode.

Keywords $Li_4Ti_5O_{12}$, phenolic-resin-based carbon, mesoporous composite, graphene

1 Introduction

As one of the most advanced rechargeable batteries, lithium-ion batteries (LIBs) have attracted tremendous attention in the past decade due to its great application potential in different fields such as electric vehicles, portable electronics, and even large-scale energy storage [1]. Although being well developed for portable electronics and other small-scale devices, there is still a need to make great efforts to further improve the energy density and stability of LIBs for their applications in electrical vehicles. The commercially available LIBs suffer from several technical issues, including unsatisfied cycling stability, capacity and safety, which require screening the alternative electrode materials [2–5]. Considerable research efforts have been made on the anode material, among which spinel $Li_4Ti_5O_{12}$ (LTO) is treated as the promising one, as it exhibits a flat voltage plateau around 1.5 V (versus Li/Li^+), which is able to inhibit the formation of SEI and in turn suppress lithium dendrite deposition on the anode surface during the charge/discharge cycling. In addition, the zero-strain characteristics of LTO ensures the excellent reversibility, the outstanding structural stability as well as the fast lithium-ion mobility, which exhibits a great potential for the realization of high-rate LIBs [6–9].

One of the critical issues associated with LTO is the low electronic conductivity ($< 10^{-13}$ S/cm), for which severe polarization and poor rate-performance would arise when it works as the electrode material. Meanwhile, the conventional micrometer-size LTO particles always deliver a low specific capacity due to the sluggish lithium migration within its bulk structure [10]. Therefore, prior to putting the LTO material into practical applications, the electrochemical performance needs to be improved. For instance, it is reported by Liu et al. that LTO with a particle size of 100 nm is prepared by the two-phase interfacial reaction (cyclohexane/water) sol-gel method. After 50 cycles, the nano-LTO still delivers a discharge capacity of 150 mAh/g and 126.6 mAh/g at 10 C and 20 C [11]. Zhu et al. designed a kind of 3D hollow LTO microspheres by hydrothermal reaction of lithium peroxotitanate complex solution and a calcination treatment. The material delivers a rate capability of 139, 125, and 108 mAh/g at 10, 20, and 30 C. After 1000 cycles at 30 C, it still has a 94% capacity retention [12]. A kind of $Li_4Ti_5O_{12}$ with a porous morphological structure is prepared by utilizing the combustion method. The capacity of particles obtained at 700°C reaches 125 mAh/g at 10 C [13]. More comparisons are listed in supplementary information.

In Refs. [14,15], carbon-coated composite materials with a mesoporous structure have been designed and

Received Jul. 8, 2021; accepted Sept. 3, 2021; online Jan. 1, 2022

Cehuang FU, Shuiyun SHEN, Ruofei WU, Xiaohui YAN, Guofeng XIA, Junliang ZHANG (✉)
Institute of Fuel Cells, Key Laboratory of Power and Machinery Engineering, School of Mechanical Engineering, Shanghai Jiao Tong University, Shanghai 200240, China
E-mail: junliang.zhang@sjtu.edu.cn

synthesized, in which the unique structure with large surface areas and large pore volumes has proven to improve the rate capability of LIBs. The important effect of the carbon coating has also been verified in Refs. [4–6]. Herein, a kind of mesoporous LTO/C composite embedded in graphene matrix (denoted as LTO/C/rGO) as the LIB anode have been proposed and designed, which consists of an LTO core, a phenolic-resin-based carbon shell, and a porous frame constructed by rGO, to facilitate the transport of both lithium ions and electrons. First, the carbon coating is formed by resol, which limits the size of the primary nanoparticles. Then, the GO is assembled by the hydrogen bond effect. Finally, the hierarchical structure is formed by the calcination process. The hierarchical structure offers unique advantages, including the increased electrode-electrolyte interfacial area and the reduced mechanical lattice strain upon lithium insertion/desertion benefited from the mesoporous carbon coated LTO, as well as the formation of a highly conductive network derived from the rGO matrix. The experimental results clearly demonstrate that the mesoporous LTO/C/rGO composite exhibits a much better rate-performance than the conventional LTOs does.

2 Experimental section

2.1 Materials

Phenol, formalin solution (37%, mass fraction), sodium hydroxide, hydrochloric acid, and ethanol were prepared by Shanghai Chemical Industrial Co., Ltd. (Shanghai, China). Tetrabutyl titanate (TBT), $CH_3COOLi \cdot 2H_2O$ (99.95%), and F127 (Pluronic block copolymer EO_{106}-PO_{70}-EO_{106}) were obtained from Sigma-Aldrich Corp.

2.2 Synthesis of Mesoporous LTO/C/rGO Composite

Figure 1 exhibits the schematic diagram of the synthesis process. In short, the carbon coating is formed by adding resol first, which limits the size of the primary nanoparticles. Then, the GO is assembled by hydrogen bond effect. Finally, the hierarchical carbon-coating structure is formed.

In detail, resol precursors (20% (mass fraction) in ethanol) could be obtained by a simple base-catalyzed process according to Refs. [15,16]. Then, the mesoporous LTO/C composite embedded in graphene matrix (LTO/C/rGO) was obtained by the co-assembly process. In brief, the molar ratio of TBT and $CH_3COOLi \cdot 2H_2O$ in the ethanol solution was about 0.85: 1. When the tetrabutyl titanate (TBT) is added into the ethanol solution, the hydrolysis reaction happens and TiO_2 is formed. Then, the LTO is synthesized by

$$5TiO_2 + 4LiOH \cdot H_2O \rightarrow Li_4Ti_5O_{12} + 6H_2O.$$

Meanwhile, 0.5 g F127 was added into the above mixture solution under strong stirring. Then, 5.28 g of TBT and 5.0 g of resol precursor solution with a certain amount of graphene oxide (GO) were added dropwise (10% of the theoretical mass of LTO) and kept stirring for 5 h. After that, the mixture was transferred to a hood at 50°C overnight, and the obtained composite was subjected to heat treatment at 120°C for 24 h. Finally, the above powder materials were calcined at 700°C in Ar atmosphere with a heating rate of 5°C/min. Using the Ar/H_2 mixture as calcination atmosphere may lead to the formation of oxygen defect [17]. Actually, the carbon will also perform reducibility in high temperature. The effect of oxygen defect on LTO was not considered.

2.3 Characterization

The morphologies and structures of the LTO composite were measured by using scanning electron microscopy (SEM, NERCN-TC-006) and transmission electron microscopy (TEM, NERCN-TC-010-1). The X-ray diffraction patterns of the above composite were recorded by the D/max-2600PC (XRD, NERCN-TC-007). Thermogravimetric analysis (TGA, NERCN-TC-013) was performed at a heating rate of 5°C/min in air atmosphere.

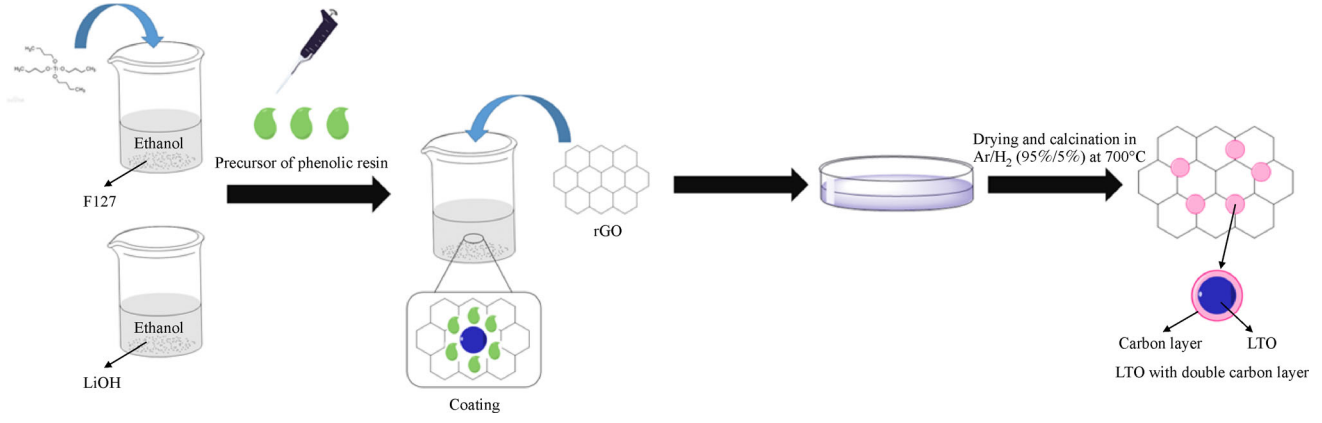

Fig. 1 Schematic diagram of the synthesis process of LTO/C/rGO.

2.4 Electrochemical testing

The electrochemical performance was tested via assembling CR2025 coin cells, which used Li metal as the counter and reference electrode. The cyclic voltammetry (CV) results were recorded on CHI760 electrochemical workstation with a scan rates of 0.1 mV/s. The galvanostatic charge/discharge performances were measured between 1.0 and 3.0 V (versus. Li^+/Li) through LAND battery stations.

2.5 Results and discussion

Figure 2(a) shows the XRD pattern of carbon-coated LTO composite (LTO/C). The characteristic peaks at 18°, 35°, 43° and 60° represent a typical LTO structure and the other two weak peaks near 25° may be ascribed to the formation of TiO_2, which has been also reported in Refs. [18,19].

Therefore, the sign of TiO_2 can be observed in the XRD data. The residual TiO_2 is unavoidable in this process. According to the weak peak in the XRD data, the content of LTO is much more than that of TiO_2. Thus, the effect of TiO_2 will not be discussed. According to the XPS data in Fig. 2(b), the characteristic peaks of Ti at 459.6 eV and 465.2 eV describe the Ti $2p_{3/2}$ and Ti $2p_{1/2}$ of Ti^{4+}. The peak at 531 eV and 532.9 eV of O 1s could be ascribed to Ti-O and C-O [20]. The XRD and XPS data suggest that the LTO is obtained successfully by the proposed method. According to the TGA results in Fig. 3, there is a main step observed after 500°C which suggests that the pure LTO composite is left. There are three stages before 500°C (0°C–100°C, 100°C–300°C and 300°C–500°C). The mass loss (about 4%) in 0°C–100°C and 100°C–300°C may come from the evaporation of the adsorbed water and crystal water. When the temperature reaches 300°C–500°C, the amorphous carbon starts to break down. rGo is added during the synthesis of LTO/C/rGO composite, for which the mass loss is more than that of the LTO/C composite. The carbon content within LTO/C and LTO/C/rGO is about 10% and 12% (mass fraction) respectively (the part of water is removed). Considering the fact that the only difference between the preparation processes of LTO/C/rGO and LTO/C is the addition of graphene, the graphene content within LTO/C/rGO is 2% (mass fraction) only.

Figure 4 demonstrates the SEM images of the LTO/C and LTO/C/rGO composites. As can be observed in Figs. 4(a) and 4(b), the prepared LTO/C composite has a spherical structure, and the corresponding particle size is about 500 nm. After the co-assembly with graphene, a

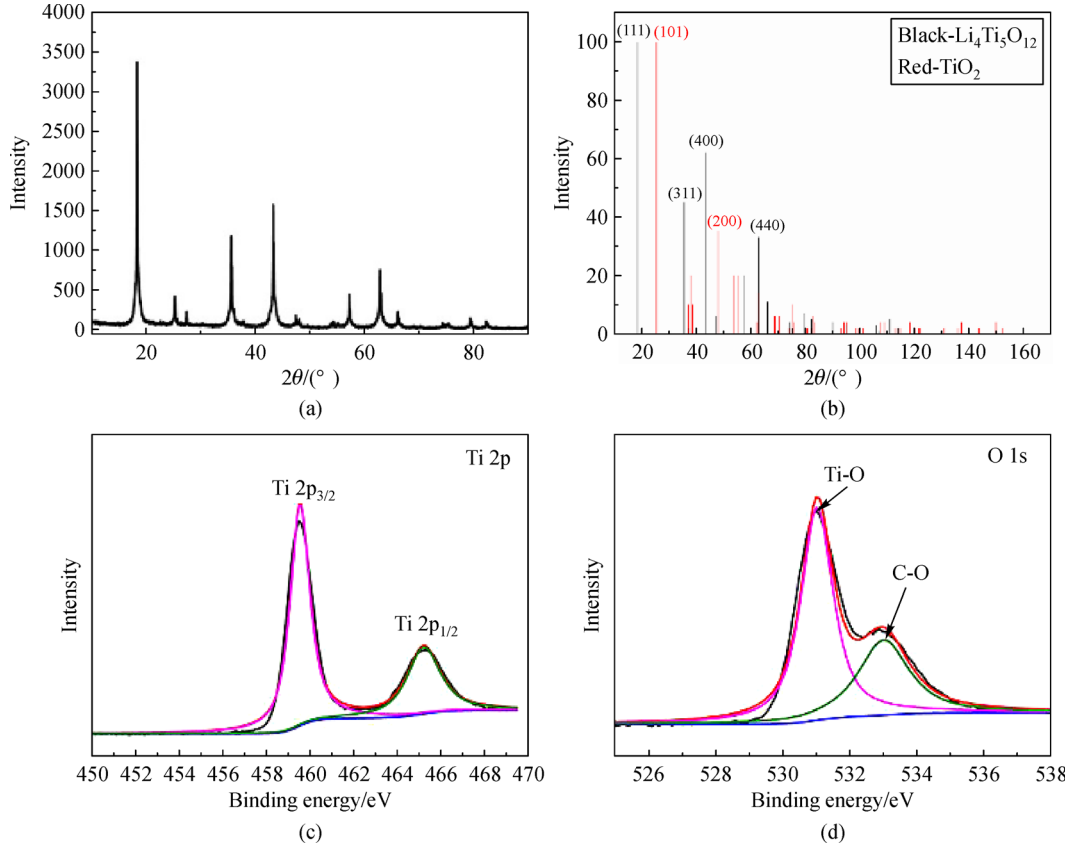

Fig. 2 Characterization data of LTO/C/rGO

(a) XRD pattern of carbon coated LTO; (b) standard XRD pattern of $Li_4Ti_5O_{12}$ and TiO_2; (c) XPS data of the Ti of LTO/C/rGO; (d) XPS data of the O of LTO/C/rGO.

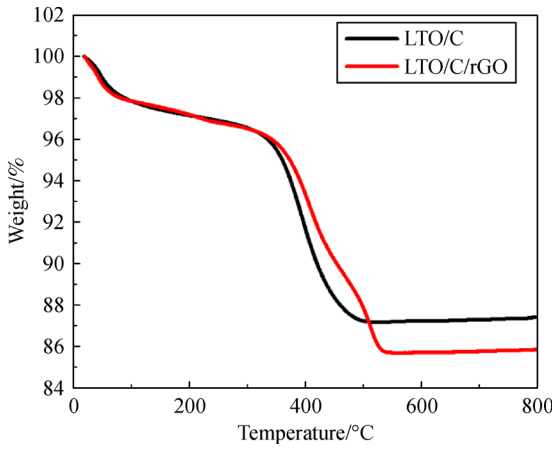

Fig. 3 TGA curves of LTO/C and LTO/C/rGO under air atmosphere at a heating rate of 5°C/min.

hierarchical structure, consisting of a LTO core, a carbon shell, and a graphene-based porous framework, could be observed in Figs. 4(c) and 4(d). It can be noticed that the LTO/C particles are closely wrapped by the rGO nanosheets. Moreover, the nanaoparticle is only 100–200 nm. The promoted structure not only improves the specific surface area and electric conductivity of LTO, but also protects the structure integrity of the composite electrode during the charge/discharge cycling [21,22].

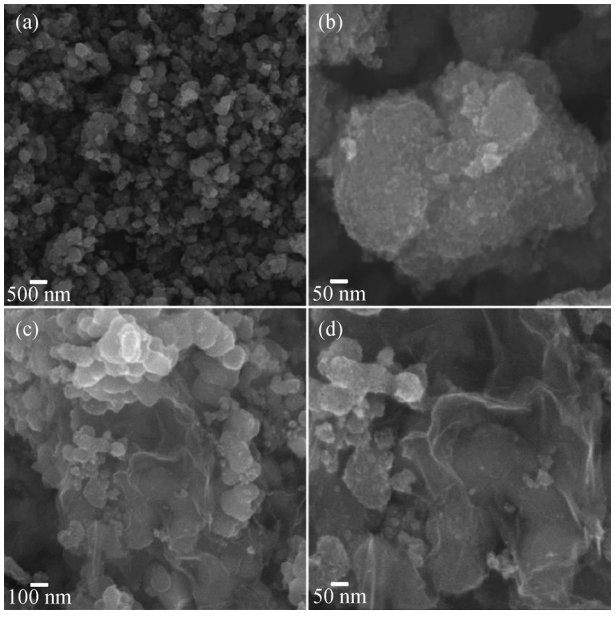

Fig. 4 Typical SEM images of LTO/C and LTO/C/rGO.
(a) LTO/C in large scale; (b) LTO/C in small scale; (c) LTO/C/rGO in large scale; (d) LTO/C/rGO in small scale.

All kinds of the LTO composites are further observed by TEM and HRTEM as manifested in Fig. 5. As can be noticed in Figs. 5(a) and 5(b), the dark and light areas come from the secondary particle of LTO/C and the amorphous carbon layers. The LTO/C composite displays a sphere shape and such large particles are packed by numerous nanoparticles, which is beneficial to form the mesoporous structure and significantly increase the surface area. In detail, the primary nanoparticles shown in Fig. 5(b) display a high LTO crystallinity with the size between 5 and 10 nm, which are coated by the amorphous carbon layers through the carbonization process of phenolic resin [23,24]. As shown in Figs. 5(c) and 5(d), a graphene area among the LTO/C composite is observed, which is consistent with the SEM characterization. As discussed above, the mesoporous LTO/C/rGO shows the potential as LIBs anode to achieve a high rate capability and a good cycling stability due to the greatly increased conductivity and electrode-electrolyte interfacial area [25,26].

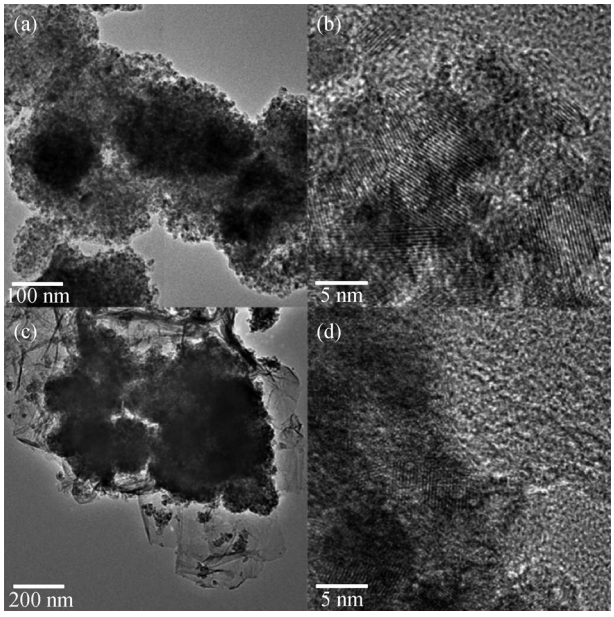

Fig. 5 Typical TEM and HRTEM images of LTO/C and LTO/C/rGO.
(a) TEM image of LTO/C; (b) HRTEM image of LTO/C; (c) TEM image of LTO/C/rGO; (d) HRTEM image of LTO/C/rGO.

To explore the electrochemical performances of LTO/C/rGO, CR2025 coin cells are assembled by using as-prepared LTO/C/rGO as the anode and Li metal as the reference electrode. Figure 6 exhibits the CV curves of the first 5 cycles at a scan rate of 0.1 mV/s. Two strong redox peaks near 1.72 V and 1.45 V are observed, which comes from the typical extraction and insertion of lithium ions within the LTO crystal. This phenomenon demonstrates the good electrode kinetics of the LTO/C/rGO electrode [27,28].

Furthermore, the capacity performance of the LTO/C/rGO composite as an anode material is evaluated by the galvanostatic charge/discharge process at different current

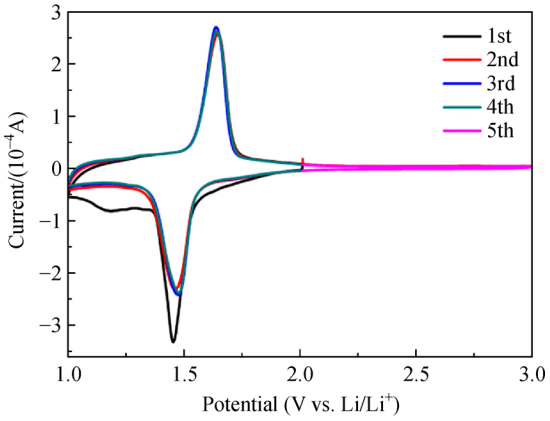

Fig. 6 CV curves of the initial 5 cycles at a scan rate of 0.1 mV/s.

densities. Figure 7 presents the typical charge/discharge profiles. The specific capacity at 0.1, 1, 2, 5, and 10 C are 175, 162, 153, 147, and 140 mAh/g, respectively. More importantly, at the high rates of 20 and 30 C, the reversible capacities still deliver high values of 127 and 119 mAh/g, which demonstrates the superior rate-performance of LTO/C/rGO.

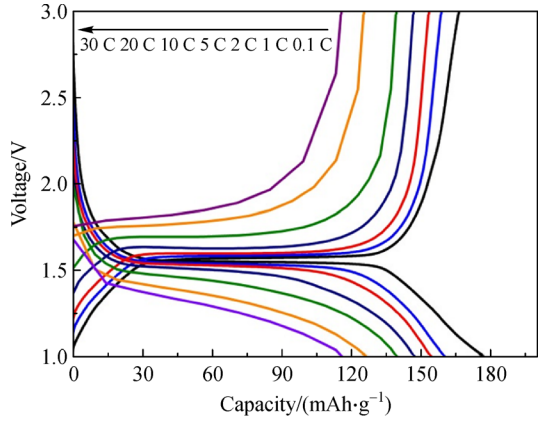

Fig. 7 Typical charge/discharge profiles of LTO/C/rGO composite at different rates.

To verify the effect of the hierarchical structure in rate capacities, different LTO samples (including bulk LTO, LTO/C, and LTO/C/rGO) are further tested at 1, 2, 5, 10, 20, and 30 C. As displayed in Fig. 8, it is remarkable that the LTO/C/rGO composite always delivers the highest capacities at each current density.

In addition, the cycling performance of the obtained LTO/C/rGO composite anode is evaluated at a high rate of 10 C. As shown in Fig. 9, there is almost no capacity decline even after 100 cycles (the Coulomb efficiency reaches the theoretical maximum), demonstrating the excellent stability of the LTO/C/rGO composite. The improved electrochemical performance could be attributed

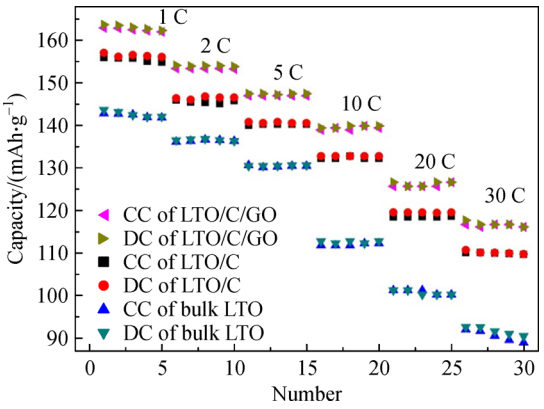

Fig. 8 Rate capacities of different electrodes when cycled at the various rates from 1 to 30 C.

to the advantages benefited from the hierarchical structure, i.e., the higher electric conductivity from the carbon-coating and graphene matrix, and the larger electrode/electrolyte interface area from the mesoporous structure.

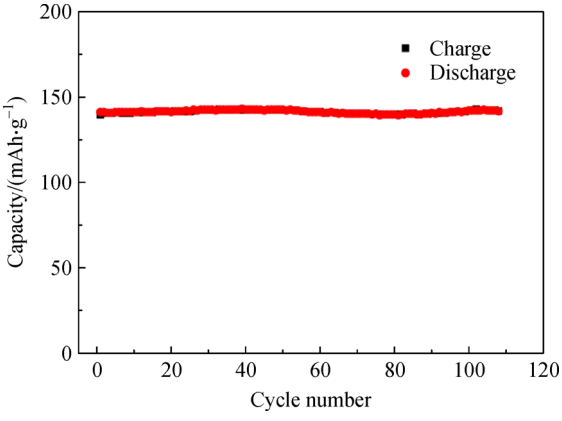

Fig. 9 Cycling performance of LTO/C/rGO composite at 10 C.

3 Conclusions

In this paper, a facile route is proposed for synthesizing mesoporous $Li_4Ti_5O_{12}$/C composite embedded in graphene matrix via the co-assembly of LTO precursor, GO, and phenolic resin. The obtained LTO/C/rGO composite presents a hierarchical structure, which makes the increased electric conductivity and electrode/electrolyte interface area possible. Due to the unique structure, the LTO/C/rGO composite exhibits a superior rate-performance, which is even able to deliver an ultrahigh capacity of 119 mAh/g at 30 C. The experimental results clearly demonstrate that the LTO/C/rGO composite material is highly suitable for the anode of high-rate LIBs.

Acknowledgements This work was supported by the National Key

Research and Development Program of China (Grant No. 2016YFB0101312) and the National Natural Science Foundation of China (Grant No. 21975157).

References

1. Jung H G, Jang M W, Hassoun J, et al. A high-rate long-life $Li_4Ti_5O_{12}$/$Li[Ni_{0.45}Co_{0.1}Mn_{1.45}]O_4$ lithium-ion battery. Nature Communications, 2011, 2(1): 516
2. Dedryvère R, Foix D, Franger S, et al. Electrode/electrolyte interface reactivity in high-voltage spinel $LiMn_{1.6}Ni_{0.4}O_4$/$Li_4Ti_5O_{12}$ lithium-ion battery. Journal of Physical Chemistry C, 2010, 114(24): 10999–11008
3. Yu H, Cao Y, Chen L, et al. Surface enrichment and diffusion enabling gradient-doping and coating of Ni-rich cathode toward Li-ion batteries. Nature Communications, 2021, 12(1): 4564
4. Deng Z, Jiang H, Li C. 2D metal chalcogenides incorporated into carbon and their assembly for energy storage applications. Small, 2018, 14(22): 1800148
5. Chen L, Liu Y, Deng Z, et al. Edge-enriched MoS_2@C/rGO film as self-standing anodes for high-capacity and long-life lithium-ion batteries. Science China Materials, 2021, 64(1): 96–104
6. Chen W, Jiang H, Hu Y, et al. Mesoporous single crystals $Li_4Ti_5O_{12}$ grown on rGO as high-rate anode materials for lithium-ion batteries. Chemical Communications: Cambridge, England, 2014, 50(64): 8856–8859
7. Huang J, Jiang Z. The preparation and characterization of $Li_4Ti_5O_{12}$/carbon nano-tubes for lithium ion battery. Electrochimica Acta, 2008, 53(26): 7756–7759
8. Liu J, Song K, van Aken P A, et al. Self-supported $Li_4Ti_5O_{12}$-C nanotube arrays as high-rate and long-life anode materials for flexible Li-ion batteries. Nano Letters, 2014, 14(5): 2597–2603
9. Yan H, Zhang D, Qilu , et al. A review of spinel lithium titanate ($Li_4Ti_5O_{12}$) as electrode material for advanced energy storage devices. Ceramics International, 2021, 47(5): 5870–5895
10. Pohjalainen E, Rauhala T, Valkeapää M, et al. Effect of $Li_4Ti_5O_{12}$ particle size on the performance of lithium ion battery electrodes at high C-rates and low temperatures. Journal of Physical Chemistry C, 2015, 119(5): 2277–2283
11. Liu G, Zhang R, Bao K, et al. Synthesis of nano-$Li_4Ti_5O_{12}$ anode material for lithium ion batteries by a biphasic interfacial reaction route. Ceramics International, 2016, 42(9): 11468–11472
12. Zhu K, Gao H, Hu G, et al. Scalable synthesis of hierarchical hollow $Li_4Ti_5O_{12}$ microspheres assembled by zigzag-like nanosheets for high rate lithium-ion batteries. Journal of Power Sources, 2017, 340: 263–272
13. Yuan T, Cai R, Wang K, et al. Combustion synthesis of high-performance $Li_4Ti_5O_{12}$ for secondary Li-ion battery. Ceramics International, 2009, 35(5): 1757–1768
14. Wu R, Shen S, Xia G, et al. Soft-templated self-assembly of mesoporous anatase TiO_2/carbon composite nanospheres for high-performance lithium ion batteries. ACS Applied Materials & Interfaces, 2016, 8(31): 19968–19978
15. Wu R, Xia G, Shen S, et al. Soft-templated $LiFePO_4$/mesoporous carbon nanosheets (LFP/meso-CNSs) nanocomposite as the cathode material of lithium ion batteries. RSC Advances, 2014, 4(41): 21325–21331
16. Meng Y, Gu D, Zhang F, et al. Ordered mesoporous polymers and homologous carbon frameworks: amphiphilic surfactant templating and direct transformation. Angewandte Chemie, 2005, 117(43): 7215–7221
17. Chen P, Cheng C, Li T, et al. Significantly improved dielectric properties of TiO_2 ceramics through acceptor-doping and Ar/H_2 annealing. Ceramics International, 2021, 47(2): 1551–1557
18. Shen L, Zhang X, Uchaker E, et al. $Li_4Ti_5O_{12}$ nanoparticles embedded in a mesoporous carbon matrix as a superior anode material for high rate lithium ion batteries. Advanced Energy Materials, 2012, 2(6): 691–698
19. Sorensen E M, Barry S J, Jung H K, et al. Three-dimensionally ordered macroporous $Li_4Ti_5O_{12}$: effect of wall structure on electrochemical properties. Chemistry of Materials, 2006, 18(2): 482–489
20. McCafferty E, Wightman J P. Determination of the concentration of surface hydroxyl groups on metal oxide films by a quantitative XPS method. Surface and Interface Analysis, 1998, 26(8): 549–564
21. Wang B, Liu T, Liu A, et al. A hierarchical porous C@$LiFePO_4$/carbon nanotubes microsphere composite for high-rate lithium-ion batteries: combined experimental and theoretical study. Advanced Energy Materials, 2016, 6(16): 1600426
22. Wang B, Al Abdulla W, Wang D, et al. A three-dimensional porous $LiFePO_4$ cathode material modified with a nitrogen-doped graphene aerogel for high-power lithium ion batteries. Energy & Environmental Science, 2015, 8(3): 869–875
23. Wu R, Xia G, Shen S, et al. *In-situ* growth of $LiFePO_4$ nanocrystals on interconnected carbon nanotubes/mesoporous carbon nanosheets for high-performance lithium ion batteries. Electrochimica Acta, 2015, 153: 334–342
24. Sun Z, Sun B, Qiao M, et al. A general chelate-assisted co-assembly to metallic nanoparticles-incorporated ordered mesoporous carbon catalysts for Fischer–tropsch synthesis. Journal of the American Chemical Society, 2012, 134(42): 17653–17660
25. Shen L, Yuan C, Luo H, et al. Facile synthesis of hierarchically porous $Li_4Ti_5O_{12}$ microspheres for high rate lithium ion batteries. Journal of Materials Chemistry, 2010, 20(33): 6998
26. Ma Y, Ding B, Ji G, et al. Carbon-encapsulated F-doped $Li_4Ti_5O_{12}$ as a high rate anode material for Li^+ batteries. ACS Nano, 2013, 7 (12): 10870–10878
27. Liu J, Song K, van Aken P A, et al. Self-supported $Li_4Ti_5O_{12}$-C nanotube arrays as high-rate and long-life anode materials for flexible Li-ion batteries. Nano Letters, 2014, 14(5): 2597–2603
28. Ding Y, Li G R, Xiao C W, et al. Insight into effects of graphene in $Li_4Ti_5O_{12}$/carbon composite with high rate capability as anode materials for lithium ion batteries. Electrochimica Acta, 2013, 102: 282–289